

Federated Learning of Nonlinear Temporal Dynamics with Graph Attention-based Cross-Client Interpretability

AYSE TURSUCULAR, AYUSH MOHANTY, NAZAL MOHAMED, NAGI GEBRAEEL,

Georgia Institute of Technology, USA

Networks of modern industrial systems are increasingly monitored by distributed sensors, where each system comprises multiple subsystems that generate high-dimensional time-series data. These subsystems are often interdependent, making it important to understand how temporal patterns observed at one subsystem relate to those observed across others. This problem is particularly challenging in decentralized settings where raw measurements cannot be shared and client observations are heterogeneous. Moreover, in many practical deployments, each subsystem (client) operates a fixed, proprietary model that cannot be modified or retrained, limiting the applicability of existing approaches. Separately, the presence of nonlinear dynamics makes cross-client temporal interdependencies inherently difficult to interpret, as they are embedded implicitly within nonlinear state-transition functions. This paper presents a federated framework for learning temporal interdependencies across clients under these constraints. Each client maps high-dimensional local observations to low-dimensional latent states using a nonlinear state-space model. A central server then learns a graph-structured neural state-transition model over the communicated latent states using a Graph Attention Network. To enable interpretability in this nonlinear setting, we relate the Jacobian of the learned server-side transition model to the attention coefficients, providing the first interpretable characterization of cross-client temporal interdependencies in decentralized nonlinear systems. We establish theoretical convergence guarantees of the proposed federated framework to a centralized oracle. We further validate the proposed framework through synthetic experiments highlighting convergence, interpretability, scalability, and privacy. Additional empirical studies on a real-world dataset demonstrate performance comparable to decentralized baselines.

1 Introduction

Modern industrial networks are increasingly monitored by distributed sensors and advanced instrumentation. In many deployments, each system consists of multiple geographically distributed subsystems [24, 27, 31] that generate high-dimensional time-series data. Despite their decentralization, these subsystems are often interdependent: localized disturbances at one subsystem can propagate across the network and affect others over time [5, 20]. Understanding such temporal interdependencies is therefore critical for system monitoring, diagnostics, and reliable operation.

In practice, these systems exhibit strongly nonlinear dynamics, making cross-subsystem temporal interdependencies vary with the system's operating state and thus difficult to interpret. While neural network models can approximate such dynamics, they typically lack structured mechanisms for exposing subsystem-level interactions. Graph-based models, particularly attention-based architectures [2, 25], provide a natural way to represent directed interactions while retaining expressive power for nonlinear dynamics.

However, centralized learning of such models is often impractical. Raw observations (data) are rarely available for centralized processing due to privacy, communication, and data-sovereignty constraints. Moreover, subsystems frequently operate fixed proprietary models supplied by original equipment manufacturers that cannot be modified or retrained [22, 23]. These constraints limit the applicability of existing centralized and decentralized approaches.

These challenges motivate a federated learning [10, 13] paradigm tailored to nonlinear dynamical systems with fixed client models. While clients cannot share raw observations or alter internal estimators, they can often communicate

Author's Contact Information: Ayse Tursucular, Ayush Mohanty, Nazal Mohamed, Nagi Gebrael, atursucular3@gatech.edu, ayush.mohanty@gatech.edu, naz@gatech.edu, nagi.gebrael@isye.gatech.edu, Georgia Institute of Technology, Atlanta, Georgia, USA.

low-dimensional latent representations of local system states. This raises a fundamental question: *can system-wide temporal interdependencies be learned from decentralized latent representations in nonlinear systems?*

Main Contribution. In this work, we answer this question by proposing a federated framework for learning temporal interdependencies in nonlinear dynamical systems with fixed proprietary client models. A Graph Attention Network-based central server learns cross-client dynamics from communicated latent states, while a Jacobian–attention analysis enables principled interpretation of how cross-client interdependencies vary with the underlying system state. To the best of our knowledge, **this is the first work to establish interpretable cross-client interdependencies in decentralized nonlinear systems**. The key technical contributions of this paper are as follows:

- We formalize federated learning of cross-client temporal interdependencies in nonlinear state-space systems with fixed proprietary client models.
- We design a GAT-parameterized server-side state-transition model over communicated latent states to explicitly represent cross-client dynamical interactions.
- We derive analytical relationships between attention coefficients and Jacobian blocks, enabling principled, state-dependent interpretation of learned interdependencies.
- We prove convergence of the learned server-side dynamics and Jacobians to a centralized oracle with access to all high-dimensional raw data.
- We empirically validate interpretability, convergence, scalability, and privacy–utility trade-offs on controlled synthetic systems, and benchmark against baselines on a real-world industrial datasets.

2 Related Work

Centralized graph neural networks (GNNs) are a standard tool for representing interdependencies among entities via message passing, ranging from early relational dynamical models such as Interaction Networks [1] to attention-based architectures that learn edge-specific importance weights [26]. For spatiotemporal interdependency modeling, many works combine graph propagation with temporal modules (RNNs/TCNs), e.g., diffusion-based recurrent models [14] and spatiotemporal graph convolutions [33]. A key thread learns the (possibly latent) interaction graph jointly with forecasting: adaptive adjacency or learned graph filters are used in traffic and multivariate forecasting [19, 29, 30]. Complementary lines infer latent interaction structure explicitly from trajectories via amortized inference, e.g., Neural Relational Inference and dynamic variants [7, 11]. These centralized methods motivate using GNNs (and attention) as representation learners for interdependency structure from time series.

Most federated GNN work studies *horizontal* partitions (clients own disjoint node/edge sets or subgraphs) and focuses on standard prediction tasks under non-IID graph distributions, often using FedAvg-style aggregation and benchmark suites [8]. Because message passing couples neighbors across partitions, several methods handle missing cross-client neighborhoods via neighbor generation or server-assisted aggregation [35, 36]. Personalized federated GNNs have also been explored, especially in recommendation-style graphs [28]. In *vertical* federated graph learning, parties split features (and sometimes edges) and coordinate secure computation for GNN layers [4, 16]; these works primarily emphasize privacy/security mechanisms and typically assume static graph data. A closely related line of work considers vertical federated learning by aligning *locally pretrained* client representations via a server-side consensus graph [15]. However, this approach does not model any client-side temporal dynamics. Our setting differs along three axes: (i) **vertical partitioning** with clients holding different views/features of the same system, (ii) the **GNN resides at the server** and clients communicate compact summaries rather than jointly running GNN layers, and (iii) **time-series (non-iid,**

temporally dependent) non-linear data is central, with the primary bottleneck being **communication/bandwidth** as the primary objective.

A separate but related literature learns directed acyclic graphs (DAGs) for causal discovery using continuous optimization, beginning with differentiable acyclicity constraints in NOTEARS [37] and nonlinear extensions using neural parameterizations [12, 34]. Interventional and likelihood-based variants improve identifiability and empirical performance [3], and temporal extensions target dynamic/lagged DAGs from time series [18]. Recent Bayesian/variational methods scale structure learning by parameterizing only acyclic graphs [9]. Federated and distributed variants adapt these ideas to multi-silo settings, e.g., federated Bayesian network structure learning via continuous optimization [17], federated DAG learning objectives [6], and adaptive federated causal discovery [32]. While these methods explicitly output a DAG (often from static or i.i.d. samples) and optimize causal scores under acyclicity, our aim is not discrete structure recovery; instead we learn a server-side GNN representation of **cross-client interdependencies in nonlinear dynamical time series** under **communication constraints** in a vertically-partitioned federation.

3 Preliminaries

3.1 Nonlinear State-Space Modeling

We consider a nonlinear state-space model (SSM) with a latent state $h_t \in \mathbb{R}^p$ and observation $y_t \in \mathbb{R}^d$. The dynamical system then evolves according to

$$h_t = f(h_{t-1}) + w_t, \quad y_t = g(h_t) + v_t, \quad (1)$$

where $f(\cdot)$ is a nonlinear *state-transition function*, $g(\cdot)$ is a nonlinear *observation function*, and w_t, v_t denote process and observation noise, respectively.

3.2 State Estimation

When the SSM is nonlinear, recursive estimation of the latent state can be performed using an Extended Kalman Filter (EKF). The EKF proceeds by alternating between a *prediction* step and an *estimation* (correction) step.

In the prediction step, the previous estimated state \hat{h}_{t-1} is propagated forward through the nonlinear dynamics to obtain a predicted state \tilde{h}_t such that,

$$\tilde{h}_t = f(\hat{h}_{t-1}), \quad (2)$$

where \tilde{h}_t represents the belief about the current state before observing y_t . In the estimation step, this prediction is updated using the new observation y_t as follows:

$$\hat{h}_t = \tilde{h}_t + K_t(y_t - g(\tilde{h}_t)), \quad (3)$$

where K_t is the Kalman gain that determines how the prediction \tilde{h}_t is corrected based on the discrepancy between the observed measurement y_t and its predicted value $g(\tilde{h}_t)$.

3.3 Jacobian for Temporal Interdependencies

To characterize directed temporal interdependencies in nonlinear dynamical systems, we decompose the latent state as $h_t = [(h_t^1)^\top, \dots, (h_t^M)^\top]^\top$ and consider its evolution under a nonlinear transition $h_t = f(h_{t-1})$.

The Jacobian $J_t = \partial f(h_{t-1}) / \partial h_{t-1}$ is a block-structured matrix whose (i, j) block captures how the j -th state component influences the i -th component over time. In this paper, we are primarily concerned with the off-diagonal

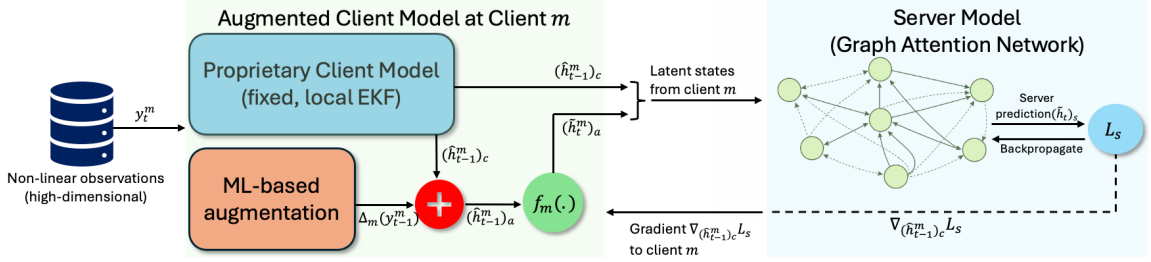


Fig. 1. Schematic of our proposed framework with communication between client m and the server

blocks:

$$J_{ij}(t) := \frac{\partial h_t^i}{\partial h_{t-1}^j}, \quad i \neq j. \quad (4)$$

The block $J_{ij}(t)$ quantifies how variations in the j -th component at time $t-1$ propagate forward to affect the i -th component at time t . As a result, the collection of off-diagonal Jacobian blocks provides a notion of directed temporal interdependencies between distinct components of the latent state in nonlinear dynamical systems.

3.4 Graph Attention Networks

Graph Attention Networks (GATs) model interdependencies among state components by combining a given graph topology with attention-based message passing. The graph specifies which components may interact, while attention mechanisms adaptively weight these interactions based on the current state.

Let $A \in \{0, 1\}^{M \times M}$ denote a given adjacency matrix, provided as input to the GAT, which encodes the graph topology. The neighborhood of each state component, denoted by $\mathcal{N}(.)$, is inferred directly from A , and determines which components participate in message passing. Given latent states $h_{t-1}^i \in \mathbb{R}^p$, a GAT layer updates each node by aggregating information from its neighbors $j \in \mathcal{N}(i)$. Each node state is first linearly transformed,

$$z_{t-1}^i = Wh_{t-1}^i, \quad (5)$$

where W is a learnable weight matrix. For each $j \in \mathcal{N}(i)$, an unnormalized attention score (*edge score*) is given by,

$$e_{ij} = a^\top \left[z_{t-1}^i \parallel z_{t-1}^j \right], \quad (6)$$

where a is a learnable vector and $[\cdot \parallel \cdot]$ denotes concatenation. The attention scores e_{ij} are then normalized across the neighborhood of node i using a softmax to obtain attention coefficients α_{ij} as,

$$\alpha_{ij} = \frac{\exp(e_{ij})}{\sum_{k \in \mathcal{N}(i)} \exp(e_{ik})}, \quad (7)$$

ensuring that $\sum_{j \in \mathcal{N}(i)} \alpha_{ij} = 1$. The resulting attention coefficients α_{ij} represent the relative contributions of neighboring state components. With $\sigma(\cdot)$ as a nonlinear activation function, the updated state is then obtained via attention-weighted aggregation as,

$$h_t^i = \sigma \left(\sum_{j \in \mathcal{N}(i)} \alpha_{ij} z_{t-1}^j \right), \quad (8)$$

4 Problem Setting

We consider a federated nonlinear dynamical system composed of M clients and a central server. At each time t , client $m \in \{1, \dots, M\}$ observes a high-dimensional observation $y_t^m \in \mathbb{R}^{d_m}$, where y_t^m denotes raw sensor data generated from an underlying low-dimensional latent state $h_t^m \in \mathbb{R}^{p_m}$, with $p_m \ll d_m$. Each client operates using only its locally available data and does not share raw observations with other clients or the server.

Furthermore, each client m is equipped with a proprietary model that estimates its latent state from local observations. For the purpose of this paper, we assume this proprietary model to be a local EKF, which produces a predicted state $(\tilde{h}_t^m)_c$ and an estimated state $(\hat{h}_t^m)_c$ at each time step t .

- **Challenge 1:** The local EKF-based state estimates $(\tilde{h}_t^m)_c$ and $(\hat{h}_t^m)_c$ depend only on client-specific dynamics, and therefore fail to capture cross-client temporal interdependencies.

Server model. To model these interdependencies, the server learns a global state-transition model over the collection of client latent states $\{(\hat{h}_t^m)_c\}_{m=1}^M$. We restrict this transition to admit a graph-structured representation parameterized by a GAT, producing server-side state predictions $(\tilde{h}_t^m)_s$ as

$$(\tilde{h}_t^m)_s = \sigma \left(\sum_{n \in N(m)} \alpha_{mn} W_{mn} (\hat{h}_{t-1}^n)_c \right), \quad (9)$$

where α_{mn} are attention coefficients and W_{mn} are learnable transformations. This model allows the server to capture directed temporal interdependencies through an explicit graph structure, rather than an unstructured black-box mapping.

- **Challenge 2:** Although the server-learned states $(\tilde{h}_t^m)_s$ capture cross-client temporal interdependencies, they cannot be directly shared with other clients. In particular, $(\tilde{h}_t^n)_s$ for $n \neq m$ are not available to client m , creating a mismatch between globally learned interdependencies and locally available state estimates.

Client model. Each client augments its proprietary EKF state using a learnable nonlinear mapping. Given the estimated state $(\hat{h}_t^m)_c$ from the proprietary model, the augmented state is given by,

$$(\hat{h}_t^m)_a = (\hat{h}_t^m)_c + \Delta_m(y_{t-1}^m; \theta_m), \quad (10)$$

where $\Delta_m(\cdot)$ denotes a learnable augmentation function. The augmentation step leaves the proprietary EKF unchanged. The augmented state evolves according to its own temporal dynamics,

$$(\tilde{h}_t^m)_a = f_m((\hat{h}_{t-1}^m)_a), \quad (11)$$

which are distinct from the proprietary EKF dynamics. Here, $(\tilde{h}_t^m)_a$ and $(\hat{h}_t^m)_a$ denote the predicted and estimated states of the augmented model, respectively.

- **Challenge 3:** Without direct access to server states $(\tilde{h}_t^n)_s$ or to raw observations $\{y_t^n\}_{n \neq m}$ from other clients, the augmented states $(\tilde{h}_t^m)_a$ cannot, on their own, learn meaningful representations of cross-client temporal interdependencies.

The communication protocol plays a central role in addressing Challenge 3. To learn the server-side GAT in (17), the server minimizes a loss L_s and communicates to each client m the gradient $\nabla_{(\tilde{h}_t^m)_a} L_s$. Each client incorporates this gradient to update the parameters of its augmentation function $\Delta_m(\cdot)$, enabling the augmented states to align with the globally learned temporal interdependencies. The iterative optimization of the GAT-based global state-transition

model at the server and the augmented models at the clients enables cross-client temporal interdependencies to be consistently encoded across the federated system.

• **Challenge 4:** Even when the server-predicted states $(\tilde{h}_t^m)_s$ and the augmented client states $(\hat{h}_t^m)_a$ are learned and well aligned, these states do not explicitly reveal which clients influence others, nor how these influences vary over time. That is, the cross-client interdependencies remain implicitly encoded in the nonlinear state-transition functions and lacks a principled interpretation.

We develop this interpretation formally using the Jacobian of the learned state-transition model in Section 6, and further analyze its implications for convergence in Sections 7. This Jacobian-based interpretability, together with the structural information provided by the attention coefficients α_{mn} 's, makes GAT a particularly well-suited choice for federated temporal interdependency learning.

5 Methodology

In this section, we describe the iterative optimization procedure between the clients and the server under privacy constraints.

5.1 Client-Side Modeling

Assumption 5.1 (Fixed Proprietary Model). Each client m maintains a proprietary EKF-based state estimator that produces a predicted state $(\tilde{h}_t^m)_c \in \mathbb{R}^{p_m}$ and a corrected state estimate $(\hat{h}_t^m)_c \in \mathbb{R}^{p_m}$ using only local observations $y_t^m \in \mathbb{R}^{d_m}$. The internal dynamics of this model are fixed and cannot be modified. Only the states $(\tilde{h}_t^m)_c$, $(\hat{h}_t^m)_c$ are available at the client.

To incorporate cross-client information without altering the proprietary model, each client augments its corrected state using a learnable nonlinear mapping

$$(\hat{h}_{t-1}^m)_a = (\hat{h}_{t-1}^m)_c + \Delta_m(y_{t-1}^m; \theta_m), \quad (12)$$

where $\Delta_m(\cdot)$ is parameterized by client-specific parameters θ_m . The augmented state follows its own temporal evolution,

$$(\tilde{h}_t^m)_a = f_m((\hat{h}_{t-1}^m)_a), \quad (13)$$

which is independent of the proprietary EKF dynamics.

Client Loss. Each client minimizes a local reconstruction loss

$$(L_m)_a = \left\| y_t^m - g_m((\tilde{h}_t^m)_a) \right\|_2^2, \quad (14)$$

where $g_m(\cdot) : \mathbb{R}^{d_m} \rightarrow \mathbb{R}^{p_m}$ is a *client-specific observation function* that maps latent states to the observation space.

The parameters θ_m are updated using gradients from both the local loss and the server loss. The server-induced gradient is computed via the chain rule,

$$\nabla_{\theta_m} L_s = \nabla_{(\tilde{h}_t^m)_a} L_s \nabla_{\theta_m} (\tilde{h}_t^m)_a, \quad (15)$$

where $\nabla_{(\tilde{h}_t^m)_a} L_s$ is received from the server.

The resulting parameter update is

$$\theta_m^{k+1} = \theta_m^k - \eta_1 \nabla_{\theta_m^k} (L_m)_a - \eta_2 \nabla_{\theta_m^k} L_s. \quad (16)$$

Client-to-Server Communication. At each communication round, client m transmits a tuple of proprietary model's states and augmented states: $((\hat{h}_t^m)_c, (\tilde{h}_t^m)_a)$ to the server.

5.2 Server-Side Graph Modeling

Assumption 5.2 (Privacy Constraint). The server neither has access to raw observations nor can it transmit latent states to clients.

The server models cross-client temporal interdependencies using a GAT. Given client states $\{(\hat{h}_t^m)_c\}_{m=1}^M$, it computes:

$$(\tilde{h}_t^m)_s = \sigma \left(\sum_{n \in \mathcal{N}(m)} \alpha_{mn} W_{mn} (\hat{h}_{t-1}^n)_c \right), \quad (17)$$

where α_{mn} are attention coefficients and W_{mn} are learnable transformations.

Server Loss. The server minimizes an MSE loss given by Eq. (18) and updates the GAT parameters via backpropagation.

$$L_s = \frac{1}{T} \sum_{t=1}^T \sum_{m=1}^M \left\| (\tilde{h}_t^m)_s - (\tilde{h}_t^m)_a \right\|_2^2, \quad (18)$$

Server-to-Client Communication. To enable learning at the clients without violating federated constraints, the server transmits to client m the gradient $\nabla_{(\tilde{h}_t^m)_a} L_s$.

Note. The use of a GAT implicitly assumes that the graph skeleton (adjacency matrix) is known *a priori*. This is reasonable in engineered systems where domain knowledge defines interconnections. The edge strengths of that graph, however, are unknown and are learned within our framework in a decentralized manner.

5.3 Method Properties

We summarize the key properties of the proposed framework, clarifying how cross-client temporal interdependencies are learned and interpreted. These properties collectively address the four challenges outlined in Section 4, and are validated in Sections 6 - 8.

Claim 5.3 (Implicit Encoding of Interdependencies). *Each client-side augmentation model $\Delta_m(\cdot)$ implicitly encodes cross-client temporal interdependencies, despite operating only on local observations y_t^m and local EKF state estimates $(\hat{h}_t^m)_c$.*

This property addresses **Challenges 1 and 3**. While the proprietary EKF estimates $(\hat{h}_t^m)_c$ depend solely on local observations and cannot capture cross-client effects, the augmentation model $\Delta_m(\cdot)$ is trained using gradients $\nabla_{(\hat{h}_t^m)_a} L_s$ communicated by the server. As a result, although evaluated only on local inputs, $\Delta_m(\cdot)$ is shaped by the global cross-client structure learned at the server.

Claim 5.4 (Alignment of Client and Server States). *The augmented client states $(\tilde{h}_t^m)_a$ and the server-predicted states $(\tilde{h}_t^m)_s$ are aligned through iterative optimization.*

In the presence of cross-client temporal interdependencies, the proprietary client states $(\hat{h}_t^m)_c$ and the server predictions $(\tilde{h}_t^m)_s$ generally differ, since the former ignore cross-client effects while the latter explicitly model them. The server loss in Eq. (18) enforces consistency between $(\tilde{h}_t^m)_s$ and $(\tilde{h}_t^m)_a$, and its gradients are propagated back to the clients to update their augmentation models. This bidirectional coupling aligns client-side and server-side state representations without sharing raw observations or server states, thereby addressing **Challenge 2**.

Claim 5.5 (Interpretable Temporal Interdependencies). *The server learns a graph-structured nonlinear state-transition model in which attention coefficients $\alpha_{mn}(t)$ regulate the aggregation of client states, and directed temporal interdependencies are characterized by the Jacobian $J_{mn}(t) = \frac{\partial(\hat{h}_t^m)_s}{\partial(\hat{h}_{t-1}^n)_c}$.*

This claim addresses **Challenge 4**. From the server transition in Eq. (17), the attention coefficients $\alpha_{mn}(t)$ quantify the relative contribution of client n 's past latent state when predicting the future state of client m . They define a directed interaction structure that governs how cross-client information is combined by the model.

However, the attention coefficients alone do not describe the resulting system dynamics. The Jacobian $J_{mn}(t)$ captures how perturbations in one client's past latent state affect another client's future state under the learned nonlinear transition. Together, $\alpha_{mn}(t)$ and $J_{mn}(t)$ provide complementary structural and dynamical views of cross-client temporal interdependencies.

6 Interpreting Temporal Interdependencies

In linear SSMs, temporal interdependencies among state components are explicitly encoded by the state-transition matrix. In nonlinear SSMs, this notion generalizes to the Jacobian of the state-transition function, which characterizes how each component of the future state locally depends on past state variables. The Jacobian therefore provides a state-dependent, directional characterization of temporal interdependencies in nonlinear dynamical systems.

In the proposed federated setting, the server-side GAT parameterizes a nonlinear state-transition function over the collection of client latent states. Two distinct but complementary quantities arise when analyzing cross-client temporal interdependencies:

- **Q1.** *Given the graph topology, how strongly is each neighbor $n \in \mathcal{N}(m)$ weighted when predicting client m 's future latent state?*
- **Q2.** *How does a perturbation in client n 's past latent state affect client m 's future latent state under the learned nonlinear dynamics?*

The question **Q1.** is addressed by the attention coefficients α_{mn} , which assign a state-dependent relative weight to each neighbor's message in the state-transition mechanism at the server. Whereas **Q2.** is addressed by the Jacobian block $J_{mn}(t) := \frac{\partial(\hat{h}_t^m)_s}{\partial(\hat{h}_{t-1}^n)_c}$, which provides a state-dependent measure of directed temporal influence.

While $\alpha_{mn}(t)$ and $J_{mn}(t)$ are related, they capture distinct aspects of cross-client temporal interdependencies. The attention coefficients $\alpha_{mn}(t)$ encode the relative structural weighting of client n 's state in the server's prediction of client m , as determined by the graph and the attention mechanism. In contrast, the Jacobian $J_{mn}(t)$ captures the resulting dynamical influence after accounting for nonlinear state evolution. Notably, the activation function $\sigma(\cdot)$ does not appear explicitly in $\alpha_{mn}(t)$, but enters the Jacobian through $\sigma'(\cdot)$, allowing nonlinear effects to modulate temporal influence. A closed-form expression of $J_{mn}(t)$ in terms of $\alpha_{mn}(t)$ is given in Proposition 6.1 below.

Proposition 6.1. *The Jacobian $J_{mn}(t)$ and the attention coefficient $\alpha_{mn}(t)$ are related as*

$$\begin{aligned} J_{mn}(t) = \text{diag}(\sigma'(s_m(t))) & \left[\alpha_{mn}(t) W_{mn} + \sum_{r \in \mathcal{N}(m)} W_{mr} \right. \\ & \times (\hat{h}_{t-1}^r)_c \alpha_{mr}(t) (\delta_{rn} - \alpha_{mn}(t)) \frac{\partial e_{mn}(t)}{\partial(\hat{h}_{t-1}^n)_c} \left. \right] \end{aligned} \quad (19)$$

where $s_m(t) := \sum_{r \in \mathcal{N}(m)} \alpha_{mr}(t) W_{mr} (\hat{h}_{t-1}^r)_c$, and δ_{rn} is the Kronecker delta.

The expression in Eq. (19) highlights two pathways through which client n can influence client m over time: **(i)** a direct pathway proportional to $\alpha_{mn}(t)W_{mn}$, and **(ii)** an indirect pathway arising from the dependence of the attention mechanism on the input states (softmax competition). As shown in Section 8, we also see that in practice, $\alpha_{mn}(t)$ and $\|J_{mn}(t)\|$ are often empirically correlated because attention controls how strongly information enters the state-transition. However, Eq. (19) depicts that the strength of this correlation depends on the activation $\sigma(\cdot)$ and the operating regime of the nonlinear dynamics.

7 Convergence Analysis

In this section, we show that the proposed federated framework converges to a centralized oracle. This validates that the learned server-side model captures the same temporal interdependencies as a fully centralized system.

Definition 7.1 (Centralized Oracle). The centralized oracle is a centralized EKF that aggregates observations from all M clients, denoted by y_o^t , to produce the predicted and estimated states \tilde{h}_o^t and \hat{h}_o^t , respectively:

$$\tilde{h}_o^t = f(\hat{h}_o^{t-1}), \quad \hat{h}_o^t = \tilde{h}_o^t + K^o(y_o^t - g(\tilde{h}_o^t)),$$

where f and g denote the nonlinear state-transition and measurement functions, respectively, and K^o is the optimal Kalman gain of the oracle. Since the vectors y_o^t , \tilde{h}_o^t , and \hat{h}_o^t , as well as the matrix K^o , contain information across all M clients, we introduce an operator $\text{Extract}_m(\cdot)$ to isolate the components of a vector or the corresponding submatrix associated with client m .

We focus on a single client (node) m with N_m neighbors and latent state dimension p_m . We assume fixed state dimensions. We further assume that the nonlinear state-transition function f of the centralized oracle admits a GAT representation. For a meaningful comparison, we restrict attention to the setting in which the oracle and the server employ the same GAT architecture and activation function σ .

At any time t , the oracle and the server update the predicted state of client m via GAT-based transitions:

$$(\tilde{h}_o^t)_m = \sigma \left(\sum_{n=1}^{N_m} \alpha_{mn}^o (\hat{h}_o^{t-1})_n \right), \quad (20)$$

$$(\tilde{h}_s^t)_m = \sigma \left(\sum_{n=1}^{N_m} \alpha_{mn}^s (\hat{h}_c^{t-1})_n \right). \quad (21)$$

Here, $\alpha_{mn}^o, \alpha_{mn}^s \in \mathbb{R}$ denote scalar attention coefficients, $(\hat{h}_o^{t-1})_n$ and $(\hat{h}_c^{t-1})_n$ denote the latent states of neighboring clients, and $\sigma : \mathbb{R}^{p_m} \rightarrow \mathbb{R}^{p_m}$ is the activation function.

Notation. Define the neighbor state matrices

$$H_o^{t-1} := \left[(\hat{h}_o^{t-1})_1 \ (\hat{h}_o^{t-1})_2 \ \cdots \ (\hat{h}_o^{t-1})_N \right] \in \mathbb{R}^{d \times N},$$

$$H_c^{t-1} := \left[(\hat{h}_c^{t-1})_1 \ (\hat{h}_c^{t-1})_2 \ \cdots \ (\hat{h}_c^{t-1})_N \right] \in \mathbb{R}^{d \times N}.$$

Let the oracle and server attention vectors be

$$\alpha_m^o := (\alpha_{m1}^o, \dots, \alpha_{mN}^o)^\top, \text{ and } \alpha_m^s := (\alpha_{m1}^s, \dots, \alpha_{mN}^s)^\top,$$

Then, $(\tilde{h}_o^t)_m = \sigma(H_o^{t-1} \alpha_m^o)$, and $(\tilde{h}_s^t)_m = \sigma(H_c^{t-1} \alpha_m^s)$.

To facilitate a convergence analysis based on matrix algebra, we impose the following assumptions:

Assumption 7.2 (Dimensionality). For each client m , the latent state dimension is significantly larger than the number of its neighbors; that is, $p_m \gg N_m$.

Assumption 7.3 (State independence). The client latent states $(\hat{h}_c^t)_m$, obtained from the local EKF-based proprietary model, are linearly independent.

We assume that the EKF dynamics used by both the centralized oracle and the proprietary client models are stable and convergent. Then the following result holds:

Lemma 7.4 (State boundedness). For sufficiently large t , there exist constants $\varepsilon_1, \varepsilon_2 \geq 0$ such that, for all clients m ,

$$\|(\tilde{h}_s^t)_m - (\hat{h}_o^t)_m\| \leq \varepsilon_1, \quad \|(\hat{h}_c^t)_m - (\hat{h}_o^t)_m\| \leq \varepsilon_2.$$

Lemma 7.4 establishes that the states predicted by both the server-side GAT and the centralized oracle remain bounded. However, bounded states alone do not guarantee that the two models induce comparable temporal interdependencies. This reflects the well-known identifiability issue in nonlinear state-space models, where distinct latent dynamics can produce indistinguishable state trajectories.

To ensure identifiability, we impose an additional regularity condition on the activation function.

Assumption 7.5 (Bi-Lipschitz activation). The activation function σ is monotone and bi-Lipschitz on the operating range; that is, there exist constants $L_\sigma, L_{\sigma^{-1}} > 0$ such that

$$\|\sigma(u) - \sigma(v)\| \leq L_\sigma \|u - v\|, \quad \|u - v\| \leq L_{\sigma^{-1}} \|\sigma(u) - \sigma(v)\|.$$

Theorem 7.6 (Bounded attention). Under the preceding assumptions, there exists a constant $C_h > 0$ such that the difference between the attention coefficients learned by the oracle and the server-side GAT is bounded as

$$\|\alpha_m^o - \alpha_m^s\| \leq \frac{C_h \varepsilon_2 + L_{\sigma^{-1}} \varepsilon_1}{\sigma_{\min}(H_c^{t-1})}.$$

Jacobian. For fixed (m, n, t) , the Jacobian of a GAT can be viewed as a mapping

$$\mathcal{J}_{mn} : (\alpha_m, H) \mapsto J_{mn}(\alpha_m, H),$$

with the server and oracle Jacobians given by

$$J_{mn}^{(s)}(t) = \mathcal{J}_{mn}(\alpha_m^s, H_c^{t-1}), \quad J_{mn}^{(o)}(t) = \mathcal{J}_{mn}(\alpha_m^o, H_o^{t-1}).$$

Explicitly, these Jacobians are defined as

$$J_{mn}^{(s)}(t) := \frac{\partial(\tilde{h}_s^t)_m}{\partial(\hat{h}_c^{t-1})_n}, \quad J_{mn}^{(o)}(t) := \frac{\partial(\tilde{h}_o^t)_m}{\partial(\hat{h}_o^{t-1})_n}.$$

Assumption 7.7 (Lipschitz continuity). There exists a constant $L_J > 0$ such that for all (α, H) and $(\tilde{\alpha}, \tilde{H})$,

$$\|\mathcal{J}_{mn}(\alpha, H) - \mathcal{J}_{mn}(\tilde{\alpha}, \tilde{H})\| \leq L_J (\|\alpha - \tilde{\alpha}\| + \|H - \tilde{H}\|_F).$$

Theorem 7.8 (Bounded Jacobian). For each fixed m and a neighboring client n , the difference between the Jacobian of the oracle and server GAT models is bounded as,

$$\|J_{mn}^{(s)}(t) - J_{mn}^{(o)}(t)\| \leq L_J \left(\frac{C_h \varepsilon_2 + L_{\sigma^{-1}} \varepsilon_1}{\sigma_{\min}(H_c^{t-1})} + \sqrt{N} \varepsilon_2 \right).$$

8 Experiments

8.1 Synthetic Dataset

We evaluate the framework on a controlled synthetic system with known ground-truth interdependencies, enabling direct validation of the method properties, interpretability questions **Q1–Q2**, and convergence analysis in Sections 5, 6, and 7, respectively. **Dataset Description.** We generate data from a nonlinear state-space system of the form

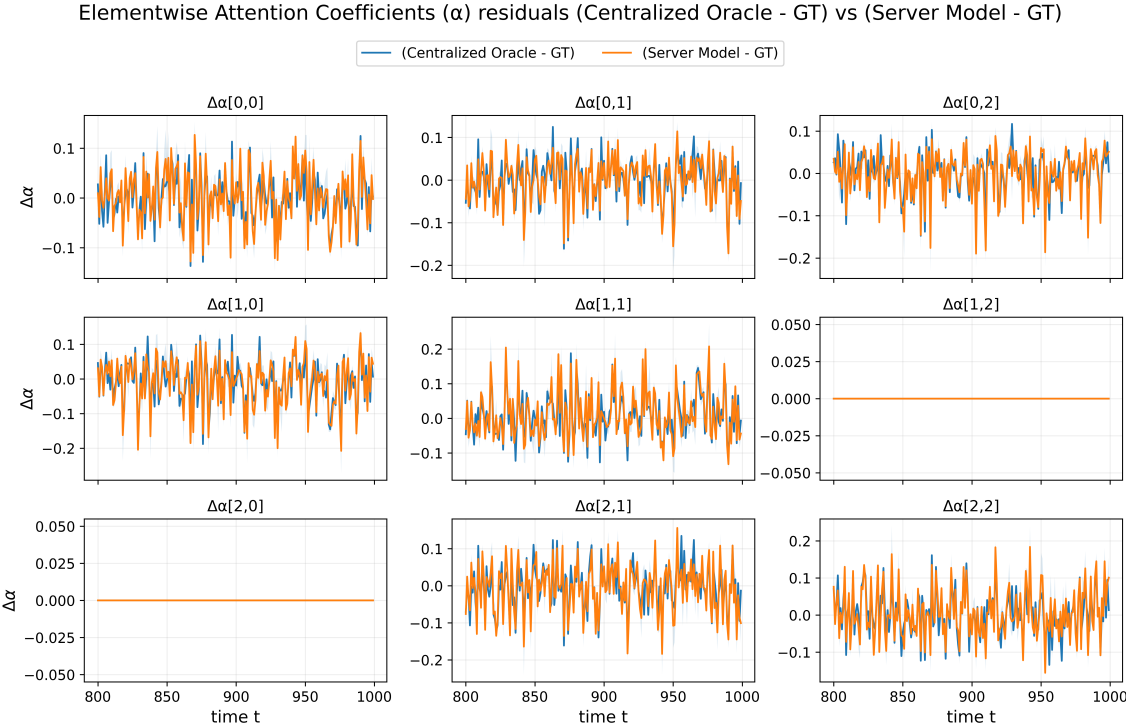


Fig. 2. Element-wise ℓ_2 norms of attention residuals relative to ground truth for the centralized and server GAT.

in Eq. (1), where the state-transition function f is implemented as a one-layer GAT with predetermined attention coefficients (serving as ground truth), the measurement function is a client-specific nonlinear mapping defined as $g_m(h_t^m) = \tanh(W_m h_t^m + b_m)$ where $W_m \in \mathbb{R}^{d_m \times p_m}$ and $b_m \in \mathbb{R}^{d_m}$ are fixed measurement parameters. We consider $M = 3$ clients with latent state dimension $p_m = 1$ and observation dimension $d_m = 8$ over $T = 1000$ time steps, using the first 800 for training and the remaining 200 for validation. All reported metrics are computed on the validation interval and averaged across runs.

Learning Cross-Client Structure. We first evaluate the framework's ability to recover the ground-truth cross-client interaction structure. To address **Q1** in Section 6, we compare the learned server-side attention coefficients $\alpha_{mn}(t)$ with the ground-truth attention used to generate the data. Figure 2 reports element-wise ℓ_2 norms of the attention residuals for the centralized oracle and the server-side GAT. The results show that the server closely matches the oracle and substantially outperforms local-only baselines. Correlation heatmaps in Figure 3 further confirms strong alignment between the learned and ground-truth attention patterns.

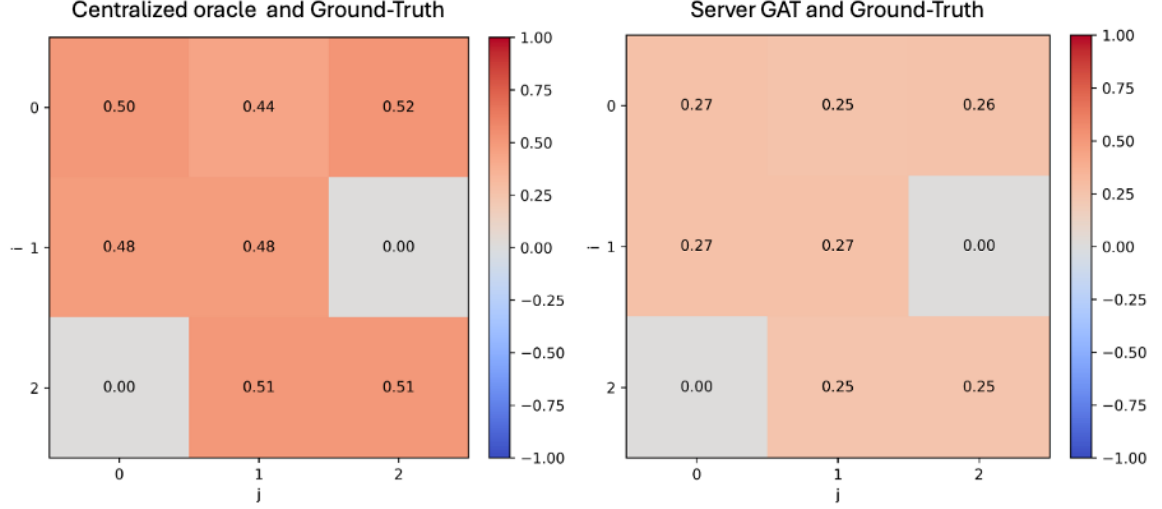


Fig. 3. Correlation between α of ground-truth GAT with centralized oracle's GAT (left), and server GAT (right).

Jacobian-Based Interpretability. To address Q2 of Section 6, we evaluate the Jacobian blocks $J_{mn}(t)$ of the learned server-side dynamics. Figure 4 reports standardized element-wise Jacobian residuals relative to ground truth, showing convergence behavior consistent with the theoretical results in Section 7. Figure 5 highlights a strong empirical correlation between attention coefficients and Jacobian magnitudes. This validates the Jacobian–attention relationship established in Proposition 6.1.

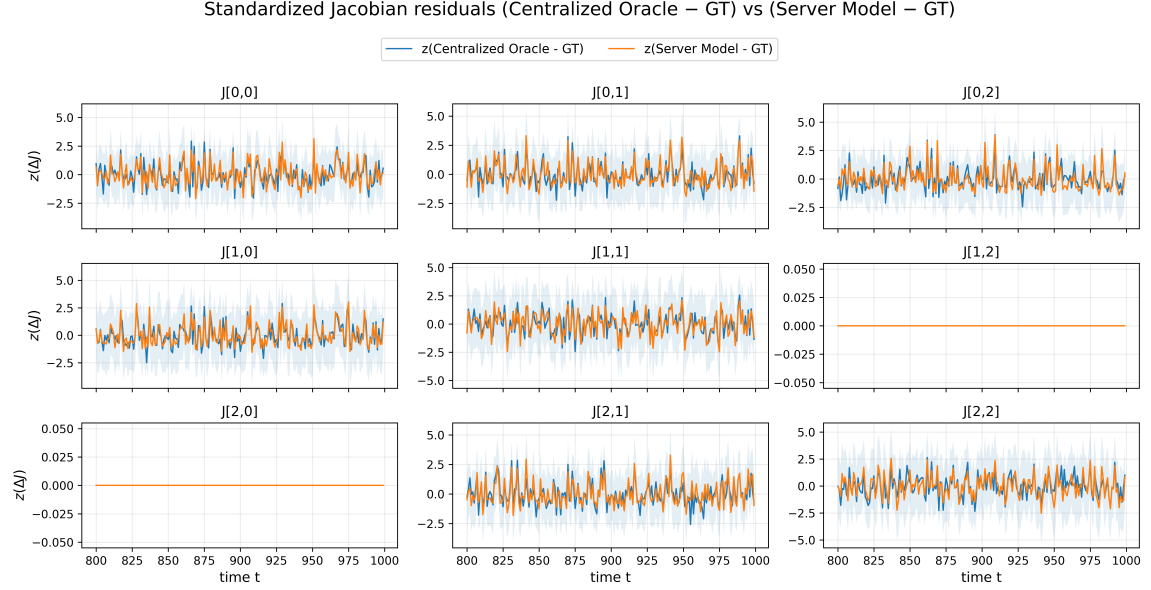


Fig. 4. Element-wise Jacobian (standardized) residuals relative to ground truth for the centralized and server GAT.

Training Dynamics. Figure 8 shows server and client loss trajectories over training, illustrating stable convergence. These results also highlight the alignment between augmented client states and server predictions, consistent with Claims 5.3–5.4. Figure 9 reports the time evolution of the validation residual norm averaged across clients. The augmented client and server models exhibit oracle-level performance, with lower residuals than the proprietary model.

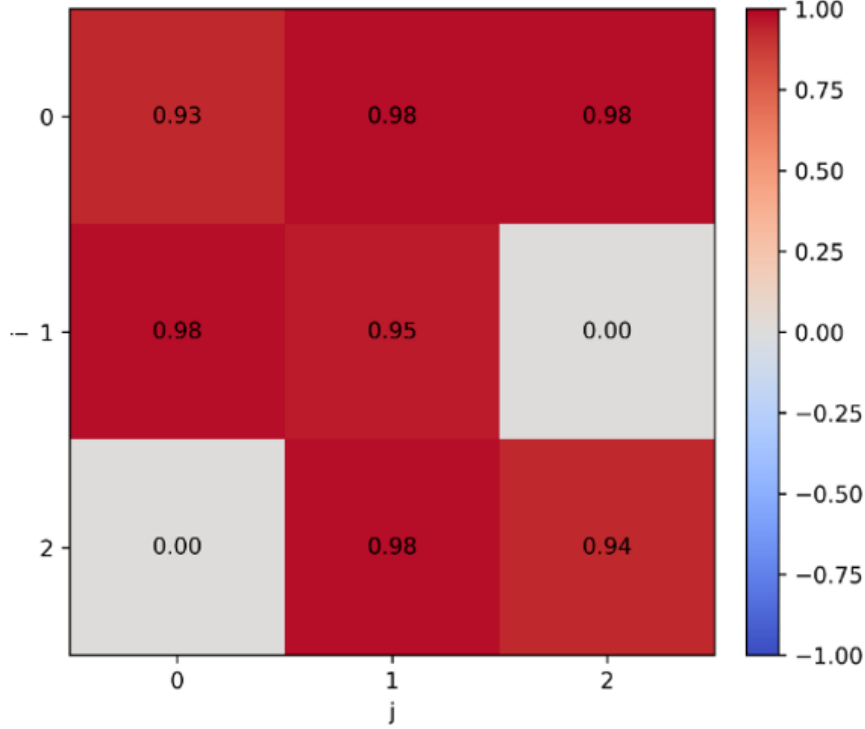


Fig. 5. Correlation between attention coefficients and Jacobian magnitudes of the server-side GAT (avg across runs).

Scalability Studies. We evaluate scalability with respect to observation dimension d_m , latent state dimension p_m , and the number of clients M , and Table 1 reports the server loss L_s as a function of communication overhead under different scalability settings. Server loss L_s is largely insensitive to observation dimension, but increases with latent dimension and number of clients due to higher communication and model complexity.

Privacy Analysis. We empirically study the privacy–utility trade-off by injecting Gaussian noise into client-to-server and server-to-client communications. Figure 10 reports the server loss L_s as a function of the client-to-server noise σ_{ca} and server-to-client noise σ_g . The results show robustness to small noise levels, with sharp degradation only at high noise, confirming a practical privacy–utility trade-off for the framework.

8.2 Real-world Dataset

We evaluate the proposed framework on a real-world industrial dataset derived from the Hardware-in-the-Loop Augmented Industrial Control System (HAI) benchmark [21], which emulates a multi-stage industrial process consisting of a water treatment process (P1), a chemical dosing process (P2), and a heating process (P3), coupled through a hardware-in-the-loop control layer (P4). Subsystems P1–P3 provide multivariate sensor measurements, while P4

Table 1. Scalability: Comm. overhead (bytes) vs. server loss.

Scale w.r.t	Comm. (in bytes)	Server loss L_s
Observation dim. d_m	32	0.0225
	64	0.0556
	128	0.0019
	256	0.0016
	512	0.0016
State dim. p_m	32	0.0019
	64	0.0103
	128	0.0859
Number of clients M	32	0.0019
	64	0.0208
	128	0.1131
	256	0.1440

contains controller and actuator signals generated by the HIL layer. Since P4 represents control logic rather than a sensing subsystem, we exclude it and treat P1, P2, and P3 as the clients.

Preprocessing. Since real-world datasets provide only sensor observations y_t^m , we apply a preprocessing step to extract low-dimensional latent states. For each client m , we perform a singular value decomposition (SVD) of the measurements y_t^m , yielding a matrix approximation of the measurement function g_m , denoted by C_{mm} . The top $p_m = 3$ right singular vectors are retained as latent states, and C_{mm} is formed from the corresponding left singular vectors and singular values. This preprocessing is applied identically to our method and all baselines, except for the centralized model.

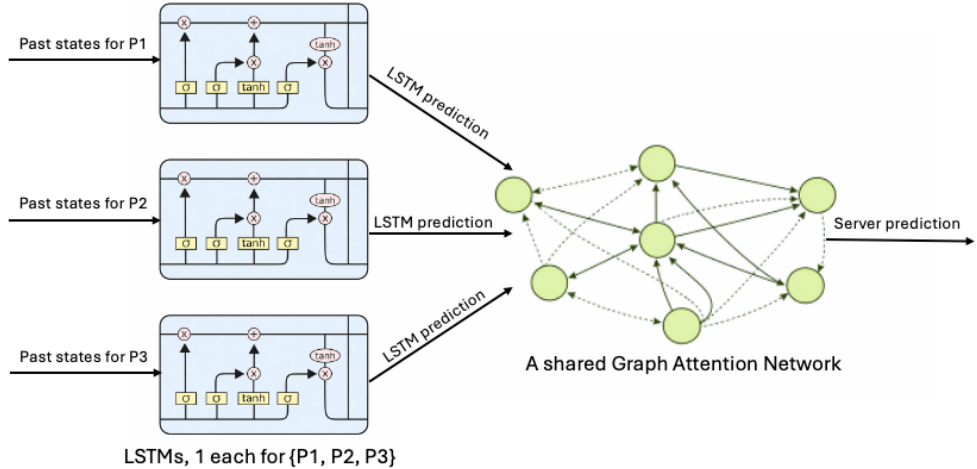


Fig. 6. Server model used for HAI dataset

Experimental Setting. Unlike the synthetic setting, real-world systems can exhibit multi-step temporal dependencies in their latent states. To capture these effects, the server uses client-specific LSTM encoders that summarize historical

latent trajectories before graph aggregation, as shown in Figure 6. Apart from this modification, the setup is identical to that used in the synthetic experiments.

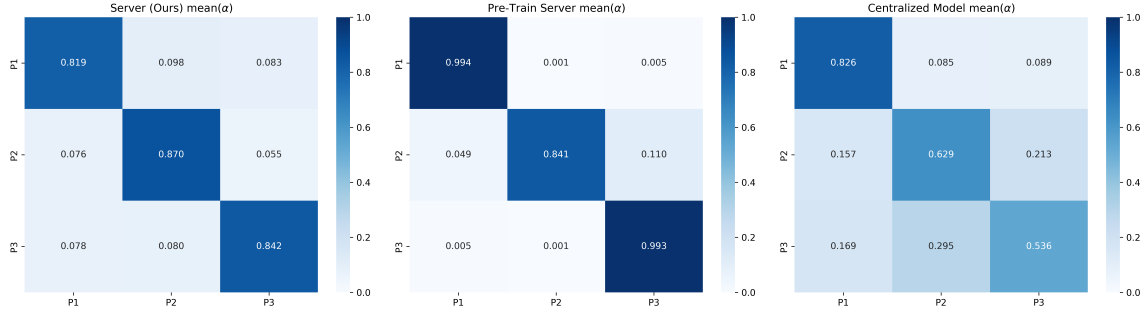


Fig. 7. Correlation of (time-averaged) attention coefficients α for the GAT used in the server of our model (left), pretrained baseline (middle), and centralized baseline (right).

Baselines. We compare against four baselines: **(i)** *Proprietary client models*, which operate locally without any federated learning; **(ii)** a *centralized* baseline with access to all client measurements, where preprocessing is performed globally by applying SVD to the concatenated observations from all clients to construct a shared low-dimensional state space; **(iii)** a *pretrained* federated baseline [15] that aligns client representations using a consensus graph but does not learn client-side dynamics; and **(iv)** *NOTEARS-ADMM* [17], a federated Bayesian network structure learning method that assumes a directed acyclic graph and operates under a horizontal federated formulation. For NOTEARS-ADMM, a global state is constructed via zero-padding of client-specific features, enabling cross-client edges but limiting the modeling of self-dynamics.

Table 2. Client and server loss comparison across baselines.

Baseline	P1	P2	P3	Avg	Server
Proprietary	0.8255	0.4817	1.0391	0.7821	–
Centralized	0.2190	0.2247	0.2440	0.2292	–
Pre-trained	–	–	–	–	0.0813
NOTEARS-ADMM	1.1815	0.8640	1.1262	1.0572	–
Our model	0.6891	0.3721	0.3308	0.4640	0.0024

Results. Figure 11 reports training loss trajectories for clients P1–P3 and the server under our model. The plots show stable optimization and consistent convergence across all components. Moreover, Figure 7 presents correlation heatmaps of time-averaged attention coefficients α_{mn} for the server GAT, comparing our model with the pretrained and centralized baseline. The attention structure learned by our model closely matches the centralized baseline, addressing **Q1** of Section 6. Additionally, Table 2 reports per-client and server losses across baselines, where our model improves client prediction accuracy over the proprietary client model (also see Table 3) and pretrained baseline while approaching centralized performance. Finally, Table 4 quantifies similarity between Jacobians learned by our server model and the centralized model, indicating strong agreement and supporting **Q2** and Claim 5.5.

9 Limitations

The framework assumes a known graph skeleton for the server-side GAT, which may be unavailable in practice and motivates integration with causal or structure discovery methods. Additionally, the Jacobian-based interpretability relies on local first-order approximations and may degrade under strong nonlinearities.

References

- [1] Peter W. Battaglia, Razvan Pascanu, Matthew Lai, Danilo Jimenez Rezende, and Koray Kavukcuoglu. 2016. Interaction Networks for Learning about Objects, Relations and Physics. In *Advances in Neural Information Processing Systems*.
- [2] Shaked Brody, Uri Alon, and Eran Yahav. 2022. How Attentive Are Graph Attention Networks?. In *International Conference on Learning Representations*.
- [3] Philippe Brouillard, Sébastien Lachapelle, Alexandre Lacoste, Simon Lacoste-Julien, and Alexandre Drouin. 2020. Differentiable causal discovery from interventional data. *Advances in Neural Information Processing Systems* 33 (2020), 21865–21877.
- [4] Chaochao Chen, Jun Zhou, Longfei Zheng, Huiwen Wu, Lingjuan Lyu, Jia Wu, Bingzhe Wu, Ziqi Liu, Li Wang, and Xiaolin Zheng. 2022. Vertically Federated Graph Neural Network for Privacy-Preserving Node Classification. In *Proceedings of the Thirty-First International Joint Conference on Artificial Intelligence*.
- [5] Lei Chen, Sergey Gorbachev, Dong Yue, Chunxia Dou, Xiangpeng Xie, Shengquan Li, Nan Zhao, and Tingjun Zhang. 2023. Impact of cascading failure on power distribution and data transmission in cyber-physical power systems. *IEEE Transactions on Network Science and Engineering* 11, 2 (2023), 1580–1590.
- [6] Erdun Gao, Junjia Chen, Li Shen, Tongliang Liu, Mingming Gong, and Howard Bondell. 2023. FedDAG: Federated DAG Structure Learning. *Transactions on Machine Learning Research* (2023).
- [7] Colin Gruber and Alexander G. Schwing. 2020. Dynamic Neural Relational Inference. In *Proceedings of the IEEE/CVF Conference on Computer Vision and Pattern Recognition*.
- [8] Chaoyang He, Keshav Balasubramanian, Emir Ceyani, Carl Yang, Han Xie, Lichao Sun, Lifang He, Liangwei Yang, Philip S. Yu, Yu Rong, Peilin Zhao, Junzhou Huang, Murali Annavaram, and Salman Avestimehr. 2021. FedGraphNN: A Federated Learning System and Benchmark for Graph Neural Networks. arXiv:2104.07145 [cs.LG] <https://arxiv.org/abs/2104.07145>
- [9] Nu T. Hoang, Bao Duong, and Thin Nguyen. 2024. Scalable Variational Causal Discovery Unconstrained by Acyclicity. In *Proceedings of the 26th European Conference on Artificial Intelligence*.
- [10] Peter Kairouz, H Brendan McMahan, Brendan Avent, Aurélien Bellet, Mehdi Bennis, Arjun Nitin Bhagoji, Kallista Bonawitz, Zachary Charles, Graham Cormode, Rachel Cummings, et al. 2021. Advances and open problems in federated learning. *Foundations and trends® in machine learning* 14, 1–2 (2021), 1–210.
- [11] Thomas N. Kipf, Ethan Fetaya, Kuan-Chieh Wang, Max Welling, and Richard Zemel. 2018. Neural Relational Inference for Interacting Systems. In *Proceedings of the 35th International Conference on Machine Learning*.
- [12] Sébastien Lachapelle, Philippe Brouillard, Tristan Deleu, and Simon Lacoste-Julien. 2020. Gradient-Based Neural DAG Learning. In *Proceedings of the Eighth International Conference on Learning Representations*.
- [13] Tian Li, Anit Kumar Sahu, Ameet Talwalkar, and Virginia Smith. 2020. Federated learning: Challenges, methods, and future directions. *IEEE signal processing magazine* 37, 3 (2020), 50–60.
- [14] Yaguang Li, Rose Yu, Cyrus Shahabi, and Yan Liu. 2018. Diffusion Convolutional Recurrent Neural Network: Data-Driven Traffic Forecasting. In *International Conference on Learning Representations*.
- [15] Tengfei Ma, Trong Nghia Hoang, and Jie Chen. 2023. Federated learning of models pre-trained on different features with consensus graphs. In *Uncertainty in artificial intelligence*. PMLR, 1336–1346.
- [16] Peihua Mai and Yan Pang. 2023. VerFedGNN: Vertical Federated Graph Neural Network for Recommender Systems. In *Proceedings of the 40th International Conference on Machine Learning*.
- [17] Ignavier Ng and Kun Zhang. 2022. Towards federated Bayesian network structure learning with continuous optimization. In *International Conference on Artificial Intelligence and Statistics*. PMLR, 8095–8111.
- [18] Roxana Pamfil, Nisara Srivattanaworachai, Shaan Desai, Philip Pilgerstorfer, Konstantinos Georgatzis, Paul Beaumont, and Bryon Aragam. 2020. DYNOTEARs: Structure Learning from Time-Series Data. In *Proceedings of the 23rd International Conference on Artificial Intelligence and Statistics*.
- [19] Chao Shang, Jie Chen, and Jimbo Bi. 2021. Discrete Graph Structure Learning for Forecasting Multiple Time Series. In *International Conference on Learning Representations*.
- [20] Dong-Hoon Shin, Dajun Qian, and Junshan Zhang. 2014. Cascading effects in interdependent networks. *Ieee Network* 28, 4 (2014), 82–87.
- [21] Hyek-Ki Shin, Woomyo Lee, Seungoh Choi, Jeong-Han Yun, and Byung-Gi Min. 2023. HAI security datasets. <https://github.com/icsdataset/hai>
- [22] Keith Stouffer, Joe Falco, Karen Scarfone, et al. 2011. Guide to industrial control systems (ICS) security. *NIST special publication 800*, 82 (2011), 16–16.
- [23] Keith Stouffer, Keith Stouffer, Michael Pease, CheeYee Tang, Timothy Zimmerman, Victoria Pillitteri, Suzanne Lightman, Adam Hahn, Stephanie Saravia, Aslam Sherule, et al. 2023. Guide to operational technology (ot) security. (2023).

- [24] Haobin Tan, Yao Xiao, Amelie Chi Zhou, Kezhong Lu, and Xuan Yang. 2025. Distributed and Adaptive Partitioning for Large Graphs in Geo-Distributed Data Centers. *IEEE Transactions on Parallel and Distributed Systems* (2025).
- [25] Petar Veličković, Guillem Cucurull, Arantxa Casanova, Adriana Romero, Pietro Liò, and Yoshua Bengio. 2018. Graph Attention Networks. In *International Conference on Learning Representations*.
- [26] Petar Veličković, Guillem Cucurull, Arantxa Casanova, Adriana Romero, Pietro Liò, and Yoshua Bengio. 2018. Graph Attention Networks. In *International Conference on Learning Representations*.
- [27] Hao Wang, Hao Luo, Lei Ren, Mingyi Huo, Yuchen Jiang, and Okyay Kaynak. 2024. Data-driven design of distributed monitoring and optimization system for manufacturing systems. *IEEE Transactions on Industrial Informatics* 20, 7 (2024), 9455–9464.
- [28] Chuhan Wu, Fangzhao Wu, Lingjuan Lyu, Tao Qi, Yongfeng Huang, and Xing Xie. 2022. A federated graph neural network framework for privacy-preserving personalization. *Nature Communications* 13, 1 (2022), 3091.
- [29] Zonghan Wu, Shirui Pan, Guodong Long, Jing Jiang, Xiaojun Chang, and Chengqi Zhang. 2020. Connecting the Dots: Multivariate Time Series Forecasting with Graph Neural Networks. In *Proceedings of the 26th ACM SIGKDD International Conference on Knowledge Discovery and Data Mining*.
- [30] Zonghan Wu, Shirui Pan, Guodong Long, Jing Jiang, and Chengqi Zhang. 2019. Graph WaveNet for Deep Spatial-Temporal Graph Modeling. In *Proceedings of the Twenty-Eighth International Joint Conference on Artificial Intelligence*.
- [31] Luolin Xiong, Anshul Goyal, Kankar Bhattacharya, Yang Tang, Zhaoyang Dong, Feng Qian, and Venkata Balaji Thummalacherla. 2025. DRL-Based Distributed Coordination of ISO and DSOs in Bi-Level Electricity Markets. *IEEE Transactions on Industrial Informatics* (2025).
- [32] Dezhui Yang, Xintong He, Jun Wang, Guoxian Yu, Carlotta Domeniconi, and Jinglin Zhang. 2024. Federated Causality Learning with Explainable Adaptive Optimization. In *Proceedings of the AAAI Conference on Artificial Intelligence*.
- [33] Bing Yu, Haoteng Yin, and Zhanxing Zhu. 2018. Spatio-Temporal Graph Convolutional Networks: A Deep Learning Framework for Traffic Forecasting. In *Proceedings of the Twenty-Seventh International Joint Conference on Artificial Intelligence*.
- [34] Yue Yu, Jie Chen, Tian Gao, and Mo Yu. 2019. DAG-GNN: DAG Structure Learning with Graph Neural Networks. In *Proceedings of the 36th International Conference on Machine Learning*.
- [35] Ke Zhang, Carl Yang, Xiaoxiao Li, Lichao Sun, and Siu Ming Yiu. 2021. Subgraph federated learning with missing neighbor generation. *Advances in neural information processing systems* 34 (2021), 6671–6682.
- [36] Longfei Zheng, Jun Zhou, Chaochao Chen, Bingzhe Wu, Li Wang, and Benyu Zhang. 2021. ASFGNN: Automated Separated-Federated Graph Neural Network. *Peer-to-Peer Networking and Applications* 14 (2021), 1692–1704.
- [37] Xun Zheng, Bryon Aragam, Pradeep K. Ravikumar, and Eric P. Xing. 2018. DAGs with NO TEARS: Continuous Optimization for Structure Learning. In *Advances in Neural Information Processing Systems*.

A Experimental Details

A.1 Additional Results on Synthetic Dataset

Details on Model Architecture. We used $M = 3$ clients with latent dimension $p_m = 1$, observation dimension $d_m = 8$, and $T = 1000$ timesteps, where observations are generated by a fixed client-specific measurement model $g_m(h_t^m) = \tanh(W_m h_t^m + b_m)$ (where $W_m \in \mathbb{R}^{d_m \times p_m}$ and $b_m \in \mathbb{R}^{d_m}$ are fixed measurement parameters) and ground-truth dynamics follow a single-layer GAT with $\tanh(\cdot)$ plus Gaussian noise (process noise standard deviation $\sigma_q = 0.05$, observation noise standard deviation $\sigma_r = 0.15$). We used a fixed adjacency matrix

$$A = \begin{bmatrix} 1 & 1 & 1 \\ 1 & 1 & 0 \\ 0 & 1 & 1 \end{bmatrix}$$

as the structural skeleton for all GAT models, such that message passing is only permitted along existing edges and no interaction is modeled where an edge is absent. Consequently, flat regions in Figure 2 are expected for non-adjacent node pairs, as the corresponding attention coefficients are masked to zero. As an oracle baseline, we used the same architecture with the ground-truth GAT as the state transition function in an Extended Kalman Filter, together with the same measurement function. The federated model uses a 1-layer server GAT and a per-client 2-layer multilayer perceptron (MLP) Δ_m (hidden size 128) for augmented state estimation, with fixed local transitions $f_m(h_t^m) = \tanh(\phi_m h_t^m)$ and $\phi = (2.0, 2.5, 3.0)$. All learnable components are trained with Adam ($\text{lr} = 10^{-3}$) for up to 200 epochs using an 80/20

time-based split and early stopping based on relative improvement of the combined training loss, with additional per-client freezing when the alignment loss plateaus.

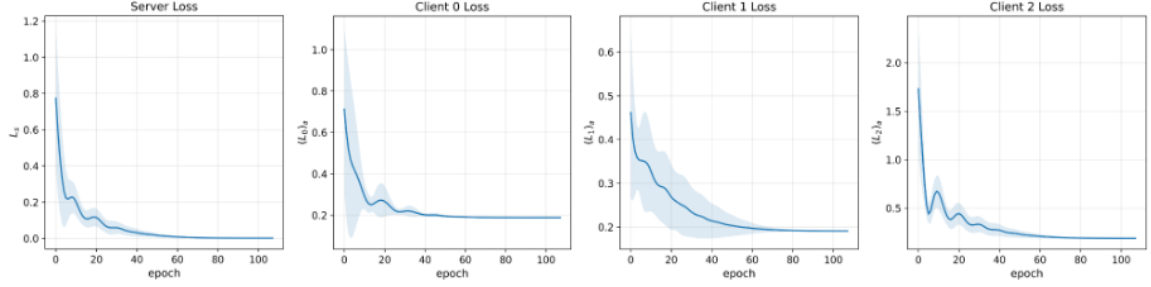


Fig. 8. Training loss curves for the server and three clients.

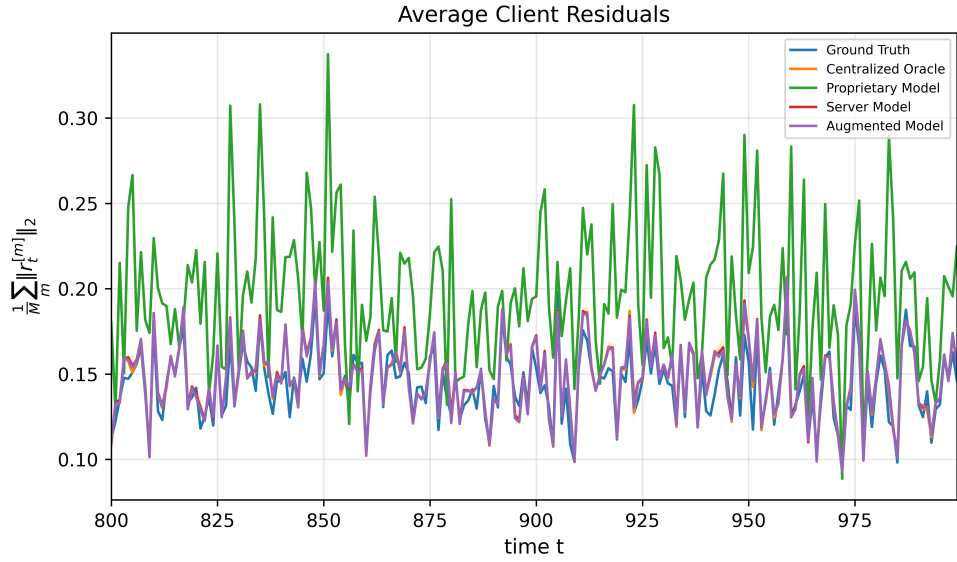


Fig. 9. Validation residual norms (avg. across all clients)

A.2 Additional Results on HAI Dataset

Proprietary Client Model. A key experimental question in our study is whether performance gains in the federated setting arise from improved modeling of inter-client dependencies, or merely from strengthening the proprietary client models themselves. To disentangle these effects, we pretrain each client’s proprietary dynamics model independently and subsequently keep these models fixed during federated training.

The HAI dataset provides two disjoint regimes: a *Nominal* dataset used for training, and an *AP04 (Attack)* dataset used for evaluation. Based on exploratory data analysis, we observe that during the AP04 attack the feedback control

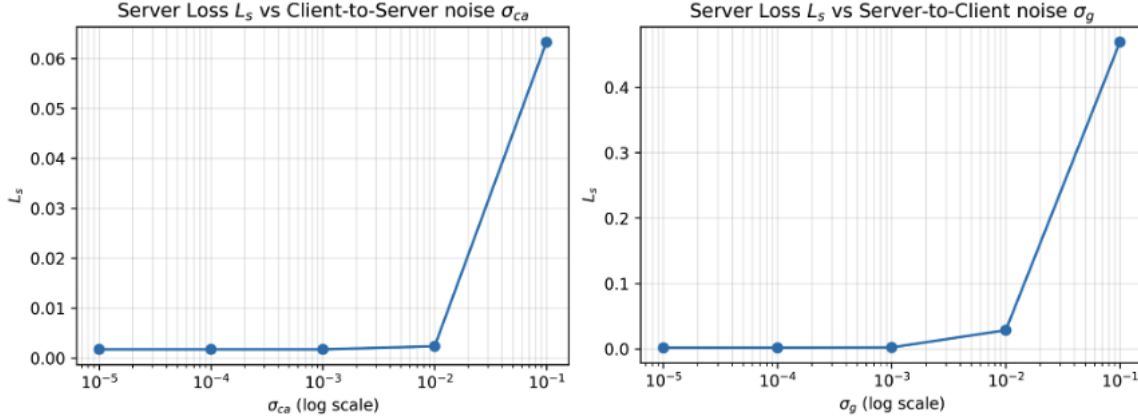


Fig. 10. Server loss L_s versus Gaussian noise during communication. Left: L_s as a function of server-to-client noise σ_g . Right: L_s as a function of client-to-server noise σ_{ca} .

mechanism is disrupted, yielding a quasi-intervention scenario in which the client subsystems (P1, P2, P3) can be treated as independently evolving for the purpose of local model training.

Specifically, for each client m , we train a local recurrent predictor f_m as a single-layer LSTM operating in a latent space of dimension p_m . We first use the *Nominal* dataset to estimate a fixed measurement operator C_{mm} via rank- p_m SVD, which captures the nominal sensor-latent structure of the system.

We then construct latent states from the *AP04 (Attack)* dataset by projecting each client's attack data onto its own rank- p_m SVD subspace. Using these latent sequences, the proprietary model f_m is trained to predict the next latent state from a history window of length S ,

$$\tilde{h}_{t,m} = f_m(\hat{h}_{t-S:t-1,m}).$$

Rather than supervising the prediction directly in latent space, we decode the predicted latent state using the fixed nominal operator C_{mm} and minimize reconstruction error in the original sensor space,

$$\mathcal{L}_{\text{prop}}^{(m)} = \left\| y_t^m - C_{mm} \tilde{h}_{t,m} \right\|_2^2.$$

This training procedure ensures that the proprietary models are learned without access to cross-client information. We train each f_m for 50 epochs using Adam with learning rate 10^{-3} and batch size 512, and subsequently freeze all proprietary model parameters for the federated learning stage.

Model Architecture and Federated Training. We consider $M = 3$ clients (P1–P3). For each client m , let $y_t^m \in \mathbb{R}^{d_m}$ denote the sensor vector at time t . All models operate with a fixed history window of length $S = 8$ and latent dimension $p_m = 3$.

Using each client's *Nominal* data, we compute a rank- p_m truncated SVD and define the corresponding right-singular subspace as a fixed linear decoder $C_{mm} \in \mathbb{R}^{d_m \times p_m}$. Nominal latent trajectories are obtained via

$$h_t^m = C_{mm}^\top y_t^m.$$

The decoder C_{mm} is held fixed throughout all experiments.

During federated training, each client learns an augmentation model Δ_m that maps a raw sensor history to a latent correction sequence. We model Δ_m as a single-layer LSTM with hidden size 64, followed by a linear head $\mathbb{R}^{64} \rightarrow \mathbb{R}^{p_m}$.

The linear head is initialized to zero so that Δ_m initially produces no correction. The augmented latent history is then passed through the frozen proprietary predictor f_m to obtain the client-side prediction.

On the server, we use an LSTM+GAT predictor that consumes latent histories and outputs a next-latent prediction \tilde{h}_t^s . The server model consists of (i) a per-client LSTM encoder over time (hidden size 64) to produce temporal embeddings, and (ii) a single-layer GAT to aggregate information across clients and predict \tilde{h}_t^s . The attention mask is given by a fixed adjacency matrix shared across all server models. We use a fully connected graph to avoid restricting potential interactions between clients.

During federated training, we optimize only the server parameters and the augmentation modules $\{\Delta_m\}_{m=1}^M$, while keeping the proprietary predictors $\{f_m\}$ frozen. We use Adam for both server and client augmentation parameters with learning rate 10^{-3} , batch size 512, and train for up to 200 epochs with 50 mini-batches per epoch. We adopt an 80/20 chronological train–test split and apply early stopping based on validation alignment loss with patience 15 and a minimum improvement threshold of 10^{-5} , restoring the best-performing server and client augmentation weights.

Centralized Baseline (Global SVD). To establish an upper-bound reference with access to all clients’ data, we implement a true centralized baseline trained on nominal data only. Unlike the federated setting, this model operates on a globally constructed latent representation and jointly optimizes predictions for all clients.

We first stack the normalized nominal sensor data from all clients horizontally, forming a global observation vector $y_t^{\text{glob}} = [y_t^1 \ y_t^2 \ y_t^3] \in \mathbb{R}^{\sum_m d_m}$. We then perform a rank- p_{glob} truncated SVD with $p_{\text{glob}} = \sum_m p_m = 9$, and define the corresponding right-singular subspace as a fixed global decoder $C_{\text{glob}} \in \mathbb{R}^{(\sum_m d_m) \times p_{\text{glob}}}$. The global latent state is obtained via $h_t^{\text{glob}} = C_{\text{glob}}^T y_t^{\text{glob}}$ and reshaped into M client-specific blocks $h_{t,m}^{\text{glob}} \in \mathbb{R}^{p_m}$.

The centralized predictor adopts the same LSTM+GAT architecture as the federated server. Given a history window $h_{t-S:t-1}^{\text{glob}}$, the model outputs a joint next-latent prediction $\tilde{h}_t^{\text{glob}} \in \mathbb{R}^{M \times p_m}$. Specifically, each client’s latent history is processed by a single-layer LSTM encoder over time (hidden size 64) to produce a temporal embedding, and these embeddings are then aggregated using a single-layer graph attention mechanism with a fully connected adjacency matrix. This design ensures unrestricted modeling of inter-client interactions.

Training is performed on the nominal dataset using an 80/20 train–test split. The predicted latent states are decoded back to the sensor space using the fixed global decoder, yielding $\hat{y}_t^{\text{glob}} = C_{\text{glob}} \tilde{h}_t^{\text{glob}}$. The model is trained by minimizing the sum of per-client reconstruction errors, $\sum_{m=1}^M \|y_t^m - \hat{y}_t^m\|_2^2$. We optimize the centralized model using Adam with learning rate 10^{-3} , batch size 512, and up to 200 epochs. Early stopping is applied based on validation reconstruction loss with patience 15 and a minimum improvement threshold of 10^{-5} , and the best-performing model parameters are restored.

This centralized model explicitly models global interdependencies under full data access. Its performance provides an upper bound against our method, augmented model.

B Proofs

B.1 Proof of Proposition 6.1

Recall the server-side GAT transition at client m :

$$(\tilde{h}_t^m)_s = \sigma(s_m(t)), \text{ with } s_m(t) := \sum_{r \in N(m)} \alpha_{mr}(t) W_{mr} (\hat{h}_{t-1}^r)_c.$$

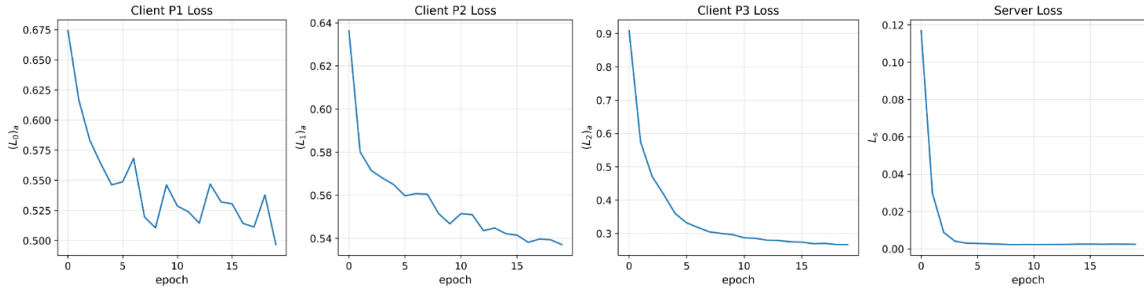


Fig. 11. Training loss for clients P1, P2, P3 and the server.

Table 3. **Relative test MSE reduction from Proprietary to Augmented model.** Percentage reduction is computed as $100 \times (\text{Proprietary} - \text{Augmented})/\text{Proprietary}$.

Client	Reduction in client loss (%)
P1	+16.53
P2	+22.74
P3	+68.16
Average	+40.67

Table 4. **Similarity metrics between the Jacobian of Server GAT of our model, and the GAT of the Centralized baseline.**

Metric	Value
Cosine Similarity	0.7277
Pearson Correlation	0.5820

Fix m, n, t and differentiate $(\hat{h}_t^m)_s$ w.r.t. $(\hat{h}_{t-1}^n)_c$. By the chain rule,

$$J_{mn}(t) := \frac{\partial(\hat{h}_t^m)_s}{\partial(\hat{h}_{t-1}^n)_c} = \text{diag}(\sigma'(s_m(t))) \frac{\partial s_m(t)}{\partial(\hat{h}_{t-1}^n)_c}. \quad (22)$$

It remains to compute $\frac{\partial s_m(t)}{\partial(\hat{h}_{t-1}^n)_c}$. Using the product rule on each summand of $s_m(t)$,

$$\frac{\partial s_m(t)}{\partial(\hat{h}_{t-1}^n)_c} = \sum_{r \in \mathcal{N}(m)} \left[\frac{\partial \alpha_{mr}(t)}{\partial(\hat{h}_{t-1}^n)_c} W_{mr} (\hat{h}_{t-1}^r)_c + \alpha_{mr}(t) W_{mr} \frac{\partial(\hat{h}_{t-1}^r)_c}{\partial(\hat{h}_{t-1}^n)_c} \right].$$

Since $\frac{\partial(\hat{h}_{t-1}^r)_c}{\partial(\hat{h}_{t-1}^n)_c} = \delta_{rn} I$, the second term yields the direct pathway $\alpha_{mn}(t)W_{mn}$. For the first term, recall that the attention coefficients are softmax-normalized:

$$\alpha_{mr}(t) = \frac{\exp(e_{mr}(t))}{\sum_{q \in \mathcal{N}(m)} \exp(e_{mq}(t))}.$$

The standard softmax derivative gives, for any $r \in \mathcal{N}(m)$,

$$\frac{\partial \alpha_{mr}(t)}{\partial e_{mn}(t)} = \alpha_{mr}(t) (\delta_{rn} - \alpha_{mn}(t)).$$

By the chain rule,

$$\frac{\partial \alpha_{mr}(t)}{\partial (\hat{h}_{t-1}^n)_c} = \frac{\partial \alpha_{mr}(t)}{\partial e_{mn}(t)} \frac{\partial e_{mn}(t)}{\partial (\hat{h}_{t-1}^n)_c} = \alpha_{mr}(t)(\delta_{rn} - \alpha_{mn}(t)) \frac{\partial e_{mn}(t)}{\partial (\hat{h}_{t-1}^n)_c}.$$

Substituting into the first term gives

$$\sum_{r \in N(m)} W_{mr} (\hat{h}_{t-1}^r)_c \alpha_{mr}(t)(\delta_{rn} - \alpha_{mn}(t)) \frac{\partial e_{mn}(t)}{\partial (\hat{h}_{t-1}^n)_c}.$$

Combining the direct and indirect contributions, we obtain

$$\begin{aligned} \frac{\partial s_m(t)}{\partial (\hat{h}_{t-1}^n)_c} &= \alpha_{mn}(t) W_{mn} + \sum_{r \in N(m)} W_{mr} (\hat{h}_{t-1}^r)_c \alpha_{mr}(t) \\ &\quad \times (\delta_{rn} - \alpha_{mn}(t)) \frac{\partial e_{mn}(t)}{\partial (\hat{h}_{t-1}^n)_c}. \end{aligned}$$

Finally, substituting this expression into (22) yields Eq. (19), proving the proposition. \square

B.2 Proof of Lemma 7.4

Assumption (Stable EKF). For each client m , assume the oracle EKF and the proprietary client EKF are mean-square stable in the following sense: there exist constants $0 < \kappa < 1$ and $B_o, B_c < \infty$ such that the corresponding estimation errors satisfy, for all t ,

$$\mathbb{E}\|(\hat{h}_o^t)_m\| \leq B_o, \quad \mathbb{E}\|(\hat{h}_c^t)_m\| \leq B_c, \quad (23)$$

and the one-step oracle prediction map is Lipschitz on the operating region. Such bounds follow from standard EKF stability results under bounded process/observation noise and local Lipschitz dynamics.

(i) Define $E_t^m := \mathbb{E}\|(\hat{h}_c^t)_m - (\hat{h}_o^t)_m\|$. Using the EKF update forms for the client and oracle and Lipschitz continuity of the observation function, we obtain a standard recursion of the form

$$E_t^m \leq a_m + b_m E_{t-1}^m, \quad \text{for some } a_m < \infty, 0 < b_m < 1, \quad (24)$$

where a_m aggregates bounded residual/noise terms, and b_m is a contraction constant determined by the local Lipschitz factors. Iterating Eq. (24) yields

$$\limsup_{t \rightarrow \infty} E_t^m \leq \frac{a_m}{1 - b_m} =: \varepsilon_2,$$

which proves the existence of $\varepsilon_2 \geq 0$ such that $\|(\hat{h}_c^t)_m - (\hat{h}_o^t)_m\| \leq \varepsilon_2$ for sufficiently large t (in expectation).

(ii) Recall the GAT equations from the paper,

$$(\tilde{h}_o^t)_m = \sigma(H_o^{t-1} \alpha_m^o), \quad (\tilde{h}_s^t)_m = \sigma(H_c^{t-1} \alpha_m^s).$$

Let $\Delta_t^m := \mathbb{E}\|(\tilde{h}_s^t)_m - (\tilde{h}_o^t)_m\|$. By Lipschitz continuity of σ and boundedness of states (23), we obtain,

$$\begin{aligned} \Delta_t^m &\leq L_\sigma \mathbb{E}\|H_c^{t-1} \alpha_m^s - H_o^{t-1} \alpha_m^o\| \\ &\leq L_\sigma \left(\mathbb{E}\|(H_c^{t-1} - H_o^{t-1}) \alpha_m^o\| + \mathbb{E}\|H_c^{t-1} (\alpha_m^s - \alpha_m^o)\| \right). \end{aligned}$$

The first term is bounded by ε_2 (since each column difference of $H_c^{t-1} - H_o^{t-1}$ is controlled by the client-oracle state gap), and the second term is bounded because H_c^{t-1} is bounded on the operating set and α_m^s, α_m^o are bounded by construction of attention (softmax). Therefore there exists $\varepsilon_1 \geq 0$ such that

$$\limsup_{t \rightarrow \infty} \Delta_t^m \leq \varepsilon_1,$$

i.e., $\|(\tilde{h}_s^t)_m - (\tilde{h}_o^t)_m\| \leq \varepsilon_1$ for sufficiently large t (in expectation). This completes the proof. \square

B.3 Proof of Theorem 7.6

Fix a client (node) m with N_m neighbors and suppress m from notation where clear. From (21) and the definitions of H_o^{t-1}, H_c^{t-1} and α_m^o, α_m^s , we can write

$$(\tilde{h}_o^t)_m = \sigma(H_o^{t-1} \alpha_m^o), \quad (\tilde{h}_s^t)_m = \sigma(H_c^{t-1} \alpha_m^s).$$

By Lemma 7.4,

$$\|\sigma(H_c^{t-1} \alpha_m^s) - \sigma(H_o^{t-1} \alpha_m^o)\| = \|(\tilde{h}_s^t)_m - (\tilde{h}_o^t)_m\| \leq \varepsilon_1.$$

Using the bi-Lipschitz inverse bound of σ (Assumption: Bi-Lipschitz),

$$\|H_c^{t-1} \alpha_m^s - H_o^{t-1} \alpha_m^o\| \leq L_{\sigma^{-1}} \varepsilon_1. \quad (25)$$

Add and subtract $H_c^{t-1} \alpha_m^o$ and apply the triangle inequality:

$$\|H_c^{t-1} \alpha_m^s - H_o^{t-1} \alpha_m^o\| \geq \|H_c^{t-1} (\alpha_m^s - \alpha_m^o)\| - \|(H_c^{t-1} - H_o^{t-1}) \alpha_m^o\|.$$

Rearranging and combining with (25) yields

$$\|H_c^{t-1} (\alpha_m^o - \alpha_m^s)\| \leq \|(H_c^{t-1} - H_o^{t-1}) \alpha_m^o\| + L_{\sigma^{-1}} \varepsilon_1. \quad (26)$$

Next, by Lemma 7.4, each neighbor column satisfies $\|(\hat{h}_c^{t-1})_n - (\hat{h}_o^{t-1})_n\| \leq \varepsilon_2$, hence there exists a constant $C_h > 0$ (depending only on $\|\alpha_m^o\|$ and N_m) such that

$$\|(H_c^{t-1} - H_o^{t-1}) \alpha_m^o\| \leq C_h \varepsilon_2. \quad (27)$$

Substituting (27) into (26) gives

$$\|H_c^{t-1} (\alpha_m^o - \alpha_m^s)\| \leq C_h \varepsilon_2 + L_{\sigma^{-1}} \varepsilon_1. \quad (28)$$

Finally, by the state-independence assumption, H_c^{t-1} has full column rank, so for any vector x , $\|H_c^{t-1} x\| \geq \sigma_{\min}(H_c^{t-1}) \|x\|$.

Applying this with $x = \alpha_m^o - \alpha_m^s$ and using (28),

$$\sigma_{\min}(H_c^{t-1}) \|\alpha_m^o - \alpha_m^s\| \leq \|H_c^{t-1} (\alpha_m^o - \alpha_m^s)\| \leq C_h \varepsilon_2 + L_{\sigma^{-1}} \varepsilon_1,$$

which implies

$$\|\alpha_m^o - \alpha_m^s\| \leq \frac{C_h \varepsilon_2 + L_{\sigma^{-1}} \varepsilon_1}{\sigma_{\min}(H_c^{t-1})}.$$

This proves Theorem 7.6. \square

B.4 Proof of Theorem 7.8

Fix a client m and a neighbor $n \in \mathcal{N}(m)$. Recall the Jacobian mapping $\mathcal{J}_{mn} : (\alpha_m, H) \mapsto J_{mn}(\alpha_m, H)$, with

$$J_{mn}^{(s)}(t) = \mathcal{J}_{mn}(\alpha_m^s, H_c^{t-1}), \quad J_{mn}^{(o)}(t) = \mathcal{J}_{mn}(\alpha_m^o, H_o^{t-1}).$$

By the Lipschitz continuity assumption on \mathcal{J}_{mn} , we have

$$\|J_{mn}^{(s)}(t) - J_{mn}^{(o)}(t)\| \leq L_J \left(\|\alpha_m^s - \alpha_m^o\| + \|H_c^{t-1} - H_o^{t-1}\|_F \right). \quad (29)$$

By Lemma 7.4 we have,

$$\|H_c^{t-1} - H_o^{t-1}\|_F = \left(\sum_{j=1}^{N_m} \|(\hat{h}_c^{t-1})_j - (\hat{h}_o^{t-1})_j\|^2 \right)^{1/2} \leq \sqrt{N_m} \varepsilon_2. \quad (30)$$

Moreover, Theorem 7.6 gives

$$\|\alpha_m^o - \alpha_m^s\| \leq \frac{C_h \varepsilon_2 + L_{\sigma^{-1}} \varepsilon_1}{\sigma_{\min}(H_c^{t-1})}. \quad (31)$$

Substituting (30) and (31) into (29) yields

$$\|J_{mn}^{(s)}(t) - J_{mn}^{(o)}(t)\| \leq L_J \left(\frac{C_h \varepsilon_2 + L_{\sigma^{-1}} \varepsilon_1}{\sigma_{\min}(H_c^{t-1})} + \sqrt{N_m} \varepsilon_2 \right),$$

which proves Theorem 7.8. \square